

**DIGITAL IMAGE CORRELATION AS
DEFORMATION MEASUREMENT TOOL IN
PLASTIC FILM BLOWING PROCESS**

KOMETHI MUNIANDY

UNIVERSITI SAINS MALAYSIA

2021

**DIGITAL IMAGE CORRELATION AS
DEFORMATION MEASUREMENT TOOL IN
PLASTIC FILM BLOWING PROCESS**

by

KOMETHI MUNIANDY

**Thesis submitted in fulfilment of the requirements
for the degree of
Doctor of Philosophy**

May 2021

ACKNOWLEDGEMENT

First and foremost, I would like to express my deepest gratitude to God for his blessings to complete my thesis of Doctor of Philosophy (Polymer Engineering).

My heartfelt gratitude goes to my supervisor, Prof. Dr. Zulkifli Mohamad Ariff, for his valuable advices, ideas, assistances and encouragements throughout my research project. He was always there to guide, supervise my research works and to provide valuable suggestions to improve the quality of my papers and thesis. My sincere appreciation to my co-supervisor, Associate Professor Dr. Azhar Abu Bakar, for his continual support, suggestions and patience to proof-read my papers and thesis without any hesitation. Special thanks to Assoc. Prof. Ir. Dr. Syed Fuad Saiyid Hashim, Dean of School of Material and Mineral Resources Engineering. Not forgetting, my thanks to all academic, administrative and technical staffs of School of Materials and Mineral Resources Engineering for their various contribution and assistance in running the research. Many thanks to Mr. Shahril Amir Saleh, Mr. Norshahrizol Nordin, Mr. Mohammad Hasan and Mr. Mohd Faizal Mohd Kassim.

My special thanks to my husband, Mr. Agilan who supported and assisted me during completion of this thesis. And most importantly, heartfelt gratitude goes to my beloved parents, Mr. Muniandy and Mrs. Devy for their blessings and constant encouragement during my years of academic achievements. So, I dedicate this thesis as an honor to them. My lovely thanks to my daughter Yuvishaa. Not forgetting my parents in law and my siblings for their greatest understanding and assistance given all these years. I do not think that I will be in this stage of my life without the support and encouragement from my family.

I would like to convey my thanks to Nur Syuhada Bt Ahmad Zauzi, Gayathirri Kuberakusalan, Navaamsini Boopalan, Nor Fasiah Bt Zaaba, Nor Anizah and all my friends for sharing their knowledge and creating a fun environment during my years of study. And a special acknowledgement to the Ministry of Higher Education for the financial support given through MyPhD scholarship which has supported me during the PhD study. Last but not least, I would like to thank all who has been directly or indirectly involved in my successful completion of my PhD project.

TABLE OF CONTENTS

ACKNOWLEDGEMENT	ii
TABLE OF CONTENTS	iii
LIST OF TABLES	vii
LIST OF FIGURES	viii
LIST OF SYMBOLS	xv
LIST OF ABBREVIATIONS	xvi
ABSTRAK	xvii
ABSTRACT	xix
CHAPTER 1 INTRODUCTION	1
1.1 Introduction.....	1
1.2 Research Problem	4
1.3 Objectives of Research	6
1.4 Thesis Outline	6
CHAPTER 2 LITERATURE REVIEW	8
2.1 Film Blowing Process.....	8
2.2 Microstructural deformation	10
2.3 In-plane Deformation.....	13
2.4 Digital Image Correlation	15
2.4.1 Basic Principle of Digital Image Correlation.....	17
2.4.2 Aspects of Measurement Accuracy	20
2.4.2(a) Pre-processing	20
2.4.2(b) Post-processing.....	21
2.5 Conventional Strain Measurement.....	22
2.5.1 Physical Gauge Measurement	22
2.5.2 Non-contact Optical Measurement	27

2.6	Recent Developments of Digital Image Correlation in Polymer Processing	31
2.6.1	Digital Image Correlation in Injection Stretch Blow Molding	31
2.6.2	Digital Image Correlation in Thermoforming	35
2.7	Versatility of Digital Image Correlation	37
CHAPTER 3 METHODOLOGY		40
3.1	Material	40
3.2	Preparation of Plastic Film	40
3.3	Film Surface Patterning	41
3.3.1	Marker types for Surface Patterning	41
3.3.2	Assessment of Surface Pattern	41
3.4	Digital Image Correlation (DIC) Analysis.....	42
3.4.1	Experimental Set-up.....	42
3.4.2	Image Acquisition	43
3.4.3	Procedure of Ncorr Open Source 2D-DIC Analysis	44
3.4.4	DIC Validation using Grid Method.....	51
3.5	Film Characterization	52
3.5.1	Measurement of Bubble Temperature.....	52
3.5.2	X-Ray Diffraction (XRD) Analysis	53
3.5.3	Differential Scanning Calorimetry	56
3.5.4	Tensile Test	57
3.5.5	Thermal Shrinkage Test	58
3.5.6	Free-falling Impact Test	60
CHAPTER 4 RESULTS AND DISCUSSION		62
4.1	Digital Image Correlation in Plastic Film Blowing Process: A Feasibility Study	62
4.1.1	Evaluation of Surface Patterning	62

4.1.1(a)	Marker types to create surface pattern	62
4.1.1(b)	Assessment of surface pattern	64
4.1.2	Deformation Analysis using Digital Image Correlation (DIC)	69
4.1.3	Validation of DIC using Grid Method	72
4.2	Optimization of DIC Parameters on the Measurement Accuracy	74
4.2.1	Effect of Subset Size	74
4.2.2	Effect of Subset Space	81
4.2.3	Effect of Strain Radius	87
4.3	Strain Progression and Structural Development during Bubble Formation.....	94
4.3.1	Thermal Properties of High-Density Polyethylene	94
4.3.2	Bubble Temperature.....	95
4.3.3	Deformation Progression of Bubble during Bubble Formation	98
4.3.4	Microstructural Development in Bubble during Bubble Formation	103
4.3.5	Relationship between strain and molecular structure.....	110
4.4	Effect of Blowing Parameters on Strain Progression and Structural Development.....	113
4.4.1	Bubble Temperature.....	113
4.4.2	Deformation Progression upon Variation in Blowing Condition.....	118
4.4.3	Microstructural Transformation upon Variation in Blowing Conditions	125
4.4.4	Thermal Properties of High-Density Polyethylene Blown Films.....	133
4.5	Thermal Deformation using Digital Image Correlation Method	137
4.5.1	Thermal Deformation as a function of Temperature.....	137
4.5.2	Proposed Structural Modification during Thermal Shrinkage	144
4.5.3	Thermal Deformation as a function of Blowing Parameters	145

4.5.4	Shrinkage measurement: DIC versus Conventional Method	155
4.6	Combination effect of film strain and molecular structure on film mechanical properties	159
4.6.1	Tensile Properties	159
4.6.2	Impact properties	171
CHAPTER 5 CONCLUSION AND FUTURE RECOMMENDATIONS ..		179
5.1	Conclusions	179
5.2	Future Recommendations	181
REFERENCES		182
LIST OF PUBLICATIONS AND CONFERENCES		

LIST OF TABLES

	Page
Table 2.1	Conventional measuring tools vs DIC24
Table 2.2.	Review on traditional video tracing method28
Table 3.1	Specification of Queens’s Film Blowing Machine40
Table 4.1	Standard deviation of grey intensities within the surface mark of four marker types66
Table 4.2	Result of displacement, strain and comparison between DIC & Grid Method73
Table 4.3	Comparison between DIC and conventional thermal shrinkage measurement158

LIST OF FIGURES

		Page
Figure 1.1	Cumulative global plastic production 1950 to 2015 (Geyer et al., 2017)	2
Figure 1.2	Global plastic production by sector (Geyer et al., 2017)	2
Figure 2.1	Film Blowing extrusion process (Wagner, 2016)	9
Figure 2.2.	Structure of semi-crystalline polymers consisting of crystalline and amorphous regions (Wietzke et al., 2010).....	11
Figure 2.3	Randomly oriented polymer chains under un-stressed state (Saeidjavash et al., 2017)	11
Figure 2.4	Row-nucleated structure of polymer chains at stressed state (Dargazany et al., 2014).....	12
Figure 2.5.	Experimental set-up (a) 2D-DIC; stereo-vision 3D-DIC using (b) single camera and set of mirrors (c) two camera (Pan et al., 2017)...	16
Figure 2.6.	Diagrams illustrates the displacement coordinates before and after deformation and the deformation parameters (Khoo et al., 2016)	18
Figure 2.7.	Bottle profile for experimental (left) and simulation (right), (a) low flow rate and (b) high flow rate (Salomeia et al., 2016)	33
Figure 2.8.	Deformation of bottle at different preform temperature (Yan et al., 2017)	34
Figure 2.9.	Typical full-field strain map, 2D and 3D illustration (hoop strain displayed) (Nixon et al., 2017).....	34
Figure 2.10.	Comparison of wall thickness between manual measurement and (a) MatchID3D (b) VIC-3D using strain form different equation (Mieghem et al., 2016)	36
Figure 3.1	(a) Stamping tool (b) Marking mechanism	43
Figure 3.2	DIC experimental set-up of film blowing process; (a) actual (b) schematic.....	43
Figure 3.3	Graphical user interface (GUI) of Ncorr loaded with reference image and current image(s).....	45
Figure 3.4	Defining the Region of Interest (ROI)	46

Figure 3.5	Selection of the DIC Parameter.....	47
Figure 3.6	Defining Initial Guess/Seed point	47
Figure 3.7	Seed placement before and after correlation process.....	49
Figure 3.8	Formatting of Displacement.....	49
Figure 3.9	Strain Computation	50
Figure 3.10	Outcome from DIC analysis	50
Figure 3.11	Regular grid patterns used in grid method, (i) reference and (ii) current image.....	51
Figure 3.12	Schematic Diagram of Bragg's Law (Thornton and Rex, 2013)	54
Figure 3.13	Diffraction peak and extractable information (Epp, 2016)	54
Figure 3.14	XRD diffraction peaks showing the area under crystalline and amorphous peaks (Lamba, 2016)	55
Figure 3.15	Dimension of dumbbell test sample type D	58
Figure 3.16	Experimental set-up for the thermal shrinkage test using digital image correlation.....	60
Figure 3.17	Pointed round head impactor	61
Figure 4.1	Types of marker used to mark the surface of blown film (a) spray paint, (b) water-based paint, (c) ink and (d) powder; (i) reference and (ii) current image	65
Figure 4.2	Grey pixel value plots of (a) ink, (b) water-based paint, (c) spray paint and (d) powder techniques; (i) reference and (ii) current image	68
Figure 4.3	Displacement contour (a) u -displacement (b) v -displacement of (i) Langrangian (ii) Eulerian of blown film	71
Figure 4.4	Strain contour (a) ϵ_{xx} (b) ϵ_{yy} of (i) Langrangian (ii) Eulerian of blown film	71
Figure 4.5	Surface pattern (a) small (b) large size with subset size of (i) 11 (ii) 15 (iii) 21 and (iv) 31 pixels.....	75
Figure 4.6	Mean intensity gradient of the surface pattern within subset size	76
Figure 4.7	Standard deviation of grey intensity of the surface pattern within subset size	77
Figure 4.8	Effect of subset size on u -displacement and v -displacement for (a) small (b) large size	79

Figure 4.9	Effect of subset size on ϵ_{xx} and ϵ_{yy} strains for Lagrangian and Eulerian position (a) small (b) large size	81
Figure 4.10	Subset space of (a) 1 (b) 3 (c) 5 pixels within a subset.....	82
Figure 4.11	Effect of subset space on u -displacement for (a) small (b) large size.....	83
Figure 4.12	Effect of subset space on v -displacement for (a) small (b) large size	84
Figure 4.13	Effect of subset space on ϵ_{xx} for (a) small (b) large size	86
Figure 4.14	Effect of subset size on ϵ_{yy} for (a) small (b) large size.....	87
Figure 4.15	Effect of strain radius on u -displacement for (a) small (b) large size.....	88
Figure 4.16	Effect of strain radius on v -displacement for (a) small (b) large size.....	89
Figure 4.17	Effect of strain radius on ϵ_{xx} for (a) small (b) large size	91
Figure 4.18	Effect of strain radius on ϵ_{yy} for (a) small (b) large size	92
Figure 4.19	Effect of strain radius (a) 1 (b) 5 (c) 9 (d) 11 (e) 15 and (f) 21 on displacement field for the small size.....	93
Figure 4.20	DSC curve of high-density polyethylene	95
Figure 4.21	Profile of bubble temperature.....	96
Figure 4.22	Line plot of bubble temperature across bubble length.....	96
Figure 4.23	Bubble temperature as a function of die distance	97
Figure 4.24	Displacements and strains progression during formation of bubble over blowing time	99
Figure 4.25	A series of strain contour in transverse direction at blowing time of (a) 30s, (b) 90s, (c) 120s, (d) 150s, (e) 180s, (f) 210s and (g) 240s	100
Figure 4.26	A series of strain contour in machine direction at blowing time of (a) 30s, (b) 90s, (c) 120s, (d) 150s, (e) 180s, (f) 210s and (g) 240s.	100
Figure 4.27	Displacements and strains progression during formation of bubble over distance from the die	102
Figure 4.28	Strain rates during bubble formation over distance from the die.....	102
Figure 4.29	XRD plot of intensity versus 2θ of HDPE resin and bubble at different axial locations from the die exit	105

Figure 4.30	XRD 2D-plot of relative intensity versus interplanar distance (d_{hkl}) of HDPE resin and bubble at different axial locations from the die exit.....	107
Figure 4.31	Interplanar distance versus distance from the die	108
Figure 4.32	Crystallinity evolution during bubble formation	109
Figure 4.33	Evolution of long period during bubble formation	110
Figure 4.34	Line plot of bubble temperature across bubble length at different (a) BUR and (b) TUR.....	115
Figure 4.35	Bubble temperature profiles at different blow up ratio (a) BUR 1.1 (b) BUR 1.6 (c) BUR 1.8 and (d) BUR 2.1	115
Figure 4.36	Bubble temperature profiles at different take up ratio (a) TUR 1.25 (b) TUR 1.50 (c) TUR 1.75 and (d) TUR 2.00	116
Figure 4.37	Bubble temperature across bubble length at different BUR	117
Figure 4.38	Bubble temperature across bubble length at different (a) BUR and (b) TUR.....	117
Figure 4.39	Progression of displacement in transverse direction over blowing time for different BUR.....	119
Figure 4.40	Progression of displacement in machine direction over blowing time for different BUR.....	119
Figure 4.41	Strain progression in transverse direction over blowing time for different BUR.....	121
Figure 4.42	Strain progression in machine direction over blowing time for different BUR.....	121
Figure 4.43	Displacement in transverse direction over blowing time for different TUR	123
Figure 4.44	Displacement in machine direction over blowing time for different TUR.....	123
Figure 4.45	Strain progression in transverse direction over blowing time for different TUR	124
Figure 4.46	Strain progression in machine direction over blowing time for different TUR	124
Figure 4.47	XRD plot of intensity versus 2θ of HDPE film at different blow up ratios.....	127

Figure 4.48	XRD plot of intensity versus 2θ of HDPE film at different take up ratios.....	128
Figure 4.49	XRD 2D-plot of relative intensity versus interplanar distance (d_{hkl}) of HDPE blown film at different blow up ratio	129
Figure 4.50	XRD 2D-plot of relative intensity versus interplanar distance (d_{hkl}) of HDPE blown film at different take up ratio.....	129
Figure 4.51	Interplanar distance (d_{hkl}) of HDPE blown film at different blowing parameter.....	130
Figure 4.52	XRD Crystallinity (%) of HDPE blown film at different blowing parameter.....	131
Figure 4.53	Long period of HDPE blown film at different blowing parameter..	132
Figure 4.54	DSC heating scans of HDPE blown films (a) BUR and (b) TUR ...	134
Figure 4.55	DSC Crystallinity (%) of HDPE blown film at different blowing parameter.....	135
Figure 4.56	DSC cooling scans of HDPE blown films (a) BUR and (b) TUR ...	136
Figure 4.57	Progression of shrinkage strain in machine direction as a function of dwell time at different shrinkage temperature	138
Figure 4.58	Progression of shrinkage strain in transverse direction as a function of dwell time at different shrinkage temperature	139
Figure 4.59	Shrinkage strain rate in machine direction as a function of dwell time at different shrinkage temperature	140
Figure 4.60	Shrinkage strain rate in transverse direction as a function of dwell time at different shrinkage temperature	140
Figure 4.61	A series of thermal strain contour in machine direction as a function of dwell time at shrinkage temperature of (a) 100 °C, (b) 110 °C, (c) 120 °C and (d) 130 °C	142
Figure 4.62	A series of thermal strain contour in transverse direction as a function of dwell time at shrinkage temperature of (a) 100 °C, (b) 110 °C, (c) 120 °C and (d) 130 °C	143
Figure 4.63	Proposed schematic diagram of structural deformation of HDPE during thermal shrinkage (Adapted from Mody et al., 2001)	145
Figure 4.64	Shrinkage strain in machine direction as a function of shrinkage time at different blow up ratio.....	146

Figure 4.65	Shrinkage strain in transverse direction as a function of shrinkage time at different blow up ratio.....	147
Figure 4.66	A series of thermal strain contour in machine direction as a function of shrinkage time at different blow up ratio; (a) 1.1, (b) 1.6, (c) 1.8 and (d) 2.1	148
Figure 4.67	A series of thermal strain contour in transverse direction as a function of shrinkage time at different blow up ratio; (a) 1.1, (b) 1.6, (c) 1.8 and (d) 2.1	149
Figure 4.68	Shrinkage strain in machine direction as a function of shrinkage time at different take up ratio	150
Figure 4.69	Shrinkage strain in transverse direction as a function of shrinkage time at different take up ratio	151
Figure 4.70	A series of thermal strain contour in machine direction as a function of shrinkage time at different take up ratio; (a) 1.25, (b) 1.5, (c) 1.75 and (d) 2.00.....	152
Figure 4.71	A series of thermal strain contour in transverse direction as a function of shrinkage time at different take up ratio; (a) 1.25, (b) 1.5, (c) 1.75 and (d) 2.0.....	153
Figure 4.72	Comparison of thermal shrinkage between conventional and DIC shrinkage measurement (a) Temperature (b) Blow up ratio (c) Take up ratio	157
Figure 4.73	Tensile strength at different blow up ratio	160
Figure 4.74	Tensile strength at different take up ratio	161
Figure 4.75	Tensile deformation in machine direction (Adapted from Callister and Rethwish, 2010)	162
Figure 4.76	Tensile deformation in transverse direction (Adapted from Cotterell et al., 2007).....	163
Figure 4.77	Correlation between film strain and tensile strength.....	164
Figure 4.78	Tensile modulus at different blow up ratio	165
Figure 4.79	Tensile modulus at different take up ratio.....	166
Figure 4.80	Correlation between film strain and tensile modulus.....	167
Figure 4.81	Elongation at break at different blow up ratio	169
Figure 4.82	Elongation at break at different take up ratio.....	169

Figure 4.83	Tendency of polymer chains to elongate upon stretching (Adapted from Azahari, 1990)	170
Figure 4.84	Correlation between film strain and elongation at break	171
Figure 4.85	Impact strength as a function of blow up ratio and take up ratio	172
Figure 4.86	Impacted crack length as a function of blow up ratio and take up ratio	174
Figure 4.87	Surface failure area as a function of blow up ratio and take up ratio	175
Figure 4.88	Impact damage at different blow up ratio and take up ration; (a) BUR 1.1, (b) BUR 1.6, (c) BUR 1.8, (d) BUR 2.1, (e) TUR 1.25, (f) TUR 1.50, (g) TUR 1.75 and (h) TUR 2.00.....	175
Figure 4.89	Impacted point and the crack path	176
Figure 4.90	Correlation between film strain ratio and impacted failure area.....	177
Figure 4.91	Correlation between film strain ratio and impacted crack length	177
Figure 4.92	Correlation between film strain ratio and impact strength.....	178

LIST OF SYMBOLS

s	second
s ⁻¹	per second
°C	Degree Celsius
mm	millimeter
cm	centimeter
nm	nanometer
mm ²	millimeter square
MPa	Mega Pascal
°	degree
%	percentage
kJ/m ²	kilo joule per meter square
d_{hkl}	Interplanar distance
u	Transverse direction displacement
v	Machine direction displacement
ϵ_{xx}	Strain in transverse direction
ϵ_{yy}	Strain in machine direction

LIST OF ABBREVIATIONS

DIC	Digital Image Correlation
BUR	Blow Up Ratio
TUR	Take Up Ratio
MD	Machine Direction
TD	Transverse Direction
MIG	Mean Intensity Gradient
SDGI	Standard Deviation of Grey Intensity
S	Subset size
FLH	Freeze Line Height

KORELASI IMEJ DIGITAL SEBAGAI ALAT PENGUKURAN DEFORMASI DALAM PROSES PENIUPAN FILEM PLASTIK

ABSTRAK

Penyelidikan ini dijalankan untuk mengkaji penggunaan korelasi imej digital (DIC) sebagai alat yang berpotensi untuk mengukur deformasi (sesaran dan terikan) semasa proses pengestrudan filem tiupan yang mampu menghasilkan pemahaman asas mengenai hubungan antara perkembangan struktur molekul dan sifat filem. Oleh itu, kajian kebolehlaksanaan kaedah DIC dari segi corak permukaan, pengesahan kaedah dan pemilihan parameter DIC telah diselidiki. Deformasi yang komprehensif dinilai menggunakan DIC untuk filem yang terbentuk dari dai hingga melepasi ketinggian garis beku (FLH) dan perkembangan struktur molekul polimer dinilai menggunakan pembelauan sinar-x (XRD). Kemajuan deformasi dan perubahan struktur mengikut nisbah tiupan (BUR) dan nisbah penarikan (TUR) telah dikaji. Kajian pengecutan termal dilakukan untuk mengkaji orientasi struktur molekul polimer amorfus. Sebagai tambahan, deformasi pengecutan terhadap permukaan filem diselidiki secara menyeluruh menggunakan DIC untuk memahami tindak balas filem terhadap haba yang mampu menggambarkan tahap deformasi yang ada dalam filem yang dihasilkan. Akhir sekali, kesan sinergi terikan dan struktur molekul terhadap sifat mekanik telah dikaji. DIC telah dibuktikan mampu menjadi kaedah yang boleh dipercayai kerana hasil yang diperoleh dengan prosedur penanda dakwat setanding dengan kaedah grid konvensional. Untuk parameter DIC, ukuran subset piksel 11 dan piksel 21 dipilih masing-masing untuk corak kecil dan besar dengan ruang subset piksel 1 dan jejari terikan piksel 5. Pembentukan gelembung semasa proses peniupan filem dapat dikelaskan kepada tiga bahagian; *parison* permulaan, pengembangan

gelembung dan melepasi ketinggian garis beku. Kesan BUR dan TUR menunjukkan bahawa filem-filem tersebut berubah secara progresif dengan nisbah tegangan. Nilai deformasi meningkat dengan nisbah tegangan kecuali dalam arah melintang (*transverse direction* – TD) yang disebabkan oleh variasi TUR. Nisbah tegangan menyebabkan perubahan minimum pada struktur filem; kehabluran, d_{hkl} dan *long period* menurun sedikit dengan nisbah tegangan. Terikan pengecutan haba dan kadar pengecutan didapati tinggi mengikut masa lengahan yang pendek pada suhu dan nisbah tegangan yang lebih tinggi. Terikan pengecutan yang lebih tinggi membuktikan kehadiran bahagian amorfus yang terorientasi lebih tinggi. Perbandingan antara pengecutan konvensional dan pengecutan DIC menunjukkan hasil yang memuaskan yang mengesahkan DIC boleh menjadi kaedah yang berguna untuk kajian ubah bentuk terma yang komprehensif. Kekuatan tegangan dan modulus tegangan pada arah menegak (*machine direction* – MD) dan arah melintang (TD) bertambah baik dengan BUR. Untuk TUR, sifat meningkat dalam MD dan menurun pada TD melebihi TUR 1.5. Secara keseluruhan, kekuatan tegangan dan modulus tegangan lebih tinggi pada MD berbanding TD. Korelasi menunjukkan sifat-sifat ini meningkat secara linear dengan ketegangan filem. Penurunan pemanjangan pada takat putus dikesan untuk BUR dan TUR. Pemanjangan pada takat putus di MD adalah lebih rendah daripada pemanjangan semasa putus di TD. Tidak ada hubungan korelasi linear yang dapat disimpulkan antara ketegangan filem dan pemanjangan semasa putus. Secara keseluruhan, dapat disimpulkan bahawa DIC dapat digunakan sebagai alat yang sesuai untuk mengukur deformasi (sesaran dan terikan) dalam proses peniupan filem plastik.

**DIGITAL IMAGE CORRELATION AS DEFORMATION
MEASUREMENT TOOL IN PLASTIC FILM BLOWING PROCESS**

ABSTRACT

The present research work investigates the use of digital image correlation (DIC) as a potential tool to measure deformation (displacement and strain) during film blowing process which can establish fundamental understanding on relationship between the structure development and film's properties. Therefore, a feasibility study of DIC method in terms of the surface patterning, validation of the method and selection of DIC parameters were investigated. The comprehensive deformation was assessed using DIC for the bubble formed exiting the die to beyond the freeze line height (FLH) and the corresponding structural development was evaluated using x-ray diffraction (XRD). The progression in deformation and the structural changes as a function of blow up ratio (BUR) and take up ratio (TUR) were studied. Thermal shrinkage study was conducted to investigate the orientation of amorphous polymer molecular structures. In addition, a comprehensive in-plane shrinkage deformation was studied using DIC to understand the response of film towards heat that could visualize the level of deformation available in the produced film. Lastly, the combination effect of the film strain and molecular structure on the mechanical properties was investigated. The DIC was proven to be a reliable method as the results obtained with the ink procedure were comparable to the conventional grid method. For the DIC parameters, subset size of 11 pixels and 21 pixels were preferred for small and large pattern, respectively with subset space of 1 pixel and strain radius of 5 pixels was chosen. The bubble formation during film blowing process can be classified into three regions; initial parison, bubble expansion and beyond freeze line height. The

effect of BUR and TUR showed that the films deformed progressively with the stretch ratios. The deformation values increase with stretching ratios except for deformation at transverse direction (TD) which caused by TUR variation. The stretch ratios caused minimal changes on film structure; the crystallinity, interplanar distance (d_{hkl}) and long period slightly reduced upon stretching ratios. The shrinkage strain and shrinkage rate found to be higher with shorter dwell time at higher temperature and stretch ratios. Higher shrinkage strain proves the presence of greater amount of oriented amorphous region. The comparison between conventional and DIC shrinkage measurement showed a satisfactory result confirming DIC can be useful method for comprehensive thermal deformation study. The tensile strength and tensile modulus in machine direction (MD) and TD improved with BUR. For TUR, the properties increased in MD and reduced for TD beyond TUR 1.5. Overall, the tensile strength and tensile modulus was higher in MD than TD. The correlation showed these properties increased linearly with the film strain. A decrease in elongation at break were detected for BUR and TUR. The elongation at break in MD was lower than the elongation at break in TD. There was no linear correlation could be deduced between film strain and elongation at break. Overall, it can be concluded that DIC can be utilized as a suitable tool to measure the deformation (displacement and strain) in plastics film blowing process.

CHAPTER 1

INTRODUCTION

1.1 Introduction

Plastic plays an important part in our daily life. The cumulative global plastic production until 2015 is 8.3 billion metric tonnes, as shown in Figure 1.1 which indicates the world has become very plastic-dependent and the plastic usage is growing (Ritchie and Roser, 2019). Plastics find their uses in various sectors as illustrated in Figure 1.2 due to their unique characteristics; inexpensive, lightweight, resilient, usually non-reactive, waterproof and durable (Hopewell et al., 2009). Plastics are dominantly used in packaging industry.

Plastics for packaging applications are generally produced using film blowing process. Film blowing process is a flexible mass production technology that produces films of different width and thickness by just adjusting process conditions which makes it a desirable process with minimal investment. Adjusting the process conditions to obtain a good film is not a trivial task. Commonly, it is a trial-and-error procedure, which could result in large wastages of material.

Present day, the world focuses on post-consumer plastic wastes, yet, tonnes of production wastages from the plastic companies have gone largely unnoticed. The production wastages are generated mainly during the processing set-up and rejections as the films failed to meet the required specifications. These wastages are usually clean and less contaminated, thus, are much easier to be recycled. Companies prefer to recycle their own scrap without leaving their facilities as it reduces the quantity of waste accumulated and the amount of virgin plastic resin requirement.

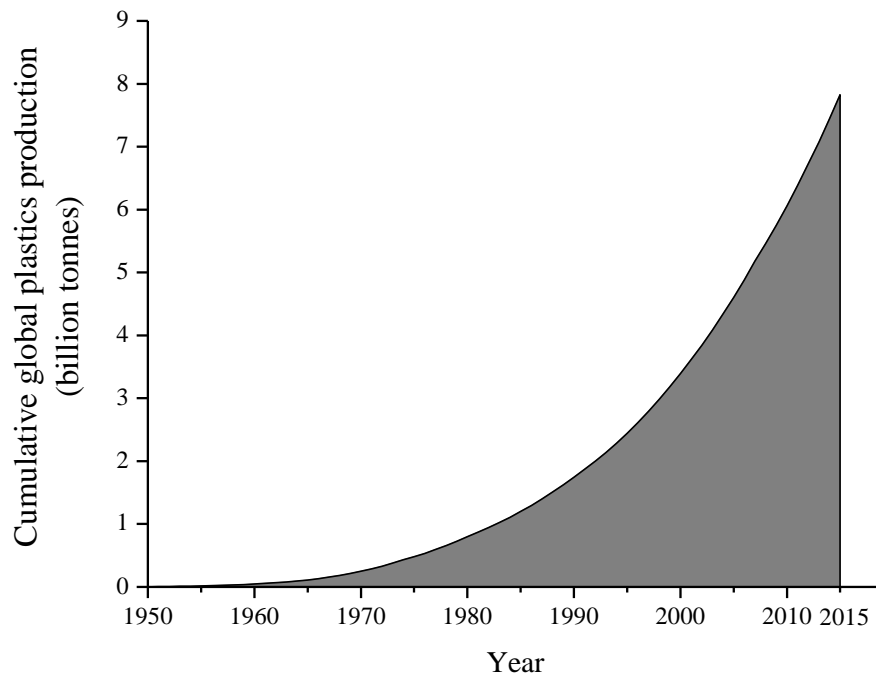


Figure 1.1 Cumulative global plastic production 1950 to 2015 (Geyer et al., 2017)

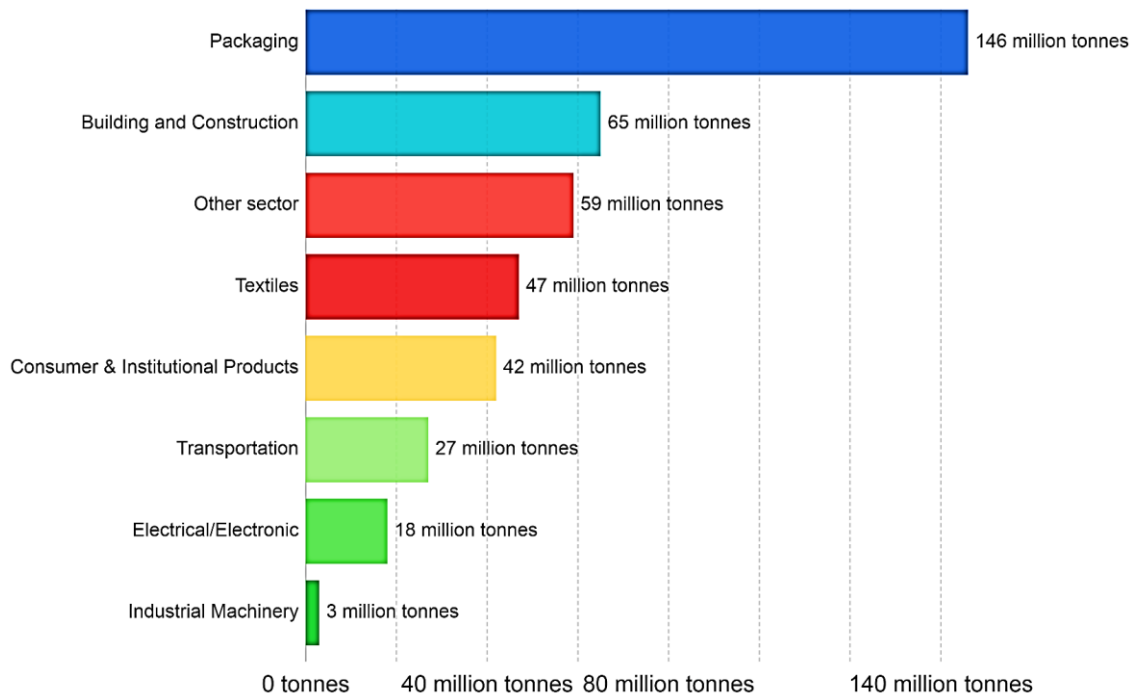


Figure 1.2 Global plastic production by sector (Geyer et al., 2017)

However, recycling is not the definite solution for the plastic companies as most plastics can only undergo limited cycles of recycling before ending up in landfills or incinerated. Besides, low commodity prices of the recycled plastics pellets discourage the recycling process. Adding to it, the production costs are lower when raw materials are used compared to the recycled plastic. It was reported that 81% of plastic manufacturing companies in Malaysia prefer for a cheaper and higher quality virgin resin rather than recycled plastic pellets (Chen et al., 2021).

Therefore, other alternative initiatives need to be implemented by the manufacturers to reduce waste as a real commitment to preserve the environment. It is crucial for the manufacturers to have the ability to predict how polymers would behave during its processing if they are to minimize wastages and yet maintain their product quality. In this research work, an attempt has made using a non-contact and non-destructive digital image correlation method to understand the response of the film during film blowing processing. Findings from this investigation is projected to able to assist manufacturers to fine tune their processing strategies so that they will have optimum processing setup and less defect (waste) during blown film manufacturing process.

Digital image correlation has been extensively investigated as a novel material characterization method in polymer processing such as injection stretch blow moulding (Yan et al., 2012; 2017, Nixon et al., 2013; 2016; 2017, Salomeia et al., 2016) and thermoforming (Mieghem et al., 2013; 2015; 2016, Ayadi et al., 2018). These research works are still under lab scale study and yet to be commercialised in polymer processing industries. Their findings explains that exploitation of DIC in the

polymer processing was able to provide original information on the deformation behaviour of polymers directly from process.

1.2 Research Problem

There is a wealth of knowledge generated by the researchers on the microstructural changes of polymers upon the processing parameter change. However, the hunt for optimum parameters is still by constant fine tuning, also known as the trial-and-error method to meet the film specification. Standard laboratory test methods are available to verify the quality of the film after the process has been completed. Post-production qualification method is laborious, time consuming and waste of material because it is a lengthy process with high accumulation of waste until the optimum parameters are found to meet the required final specification. Thus, online qualification during the processing is necessary in optimising processing parameter to reduce material waste; raw material and rejected plastic film rolls.

Therefore, a faster and reliable measurement method during the processing is needed to qualify the film by omitting the dependency on post-production qualification procedures and immediate optimization of processing parameter reducing material waste. Deformation is directly related to the strain. Physical gauges such as extensometer and electrical resistance strain gage are extensively practised in measuring the strain of deformed polymer samples. These tools provide a very reliable and accurate measurement readings. Unfortunately, it is very challenging to use these tools in plastic film blowing process as the film is very thin and moves upwards at a relatively high-speed while being stretched and deformed.

To tackle the problem, a non-contact and non-destructive digital image correlation method is proposed to understand the response of the film during processing. This research work which focuses on strain determination during plastic film blowing process is in accordance to Bing Pan's reliability guided method (Pan, 2009, Blaber et al., 2015). The use of DIC technique guides the project to a certain extent towards mapping the real way of how the material deforms and the obtained final strain can be directly related to the final film properties. This approach will benefit the industry and result in better production optimisation without the time, labour and cost consuming experimental works. This will help the industries to find fast and reliable ways of detecting and preventing failures before the product is being produced as well as finding tools to characterize post-process failures.

Additionally, the approach will give better insight to blown film manufacturers in managing their resources through knowledge-based processing strategies with the help of projected quantitative correlation between polymer flow and film failure. This will subsequently improve product quality and reliability of plastic films hence reducing unwanted production rejects. The projected reduction of waste or rejects would benefit the manufacturer in the long run and indirectly support the effort of managing solid waste throughout the nation.

1.3 Objectives of Research

The main aim of the research work is to investigate a faster and reliable measurement method to measure film deformation which is expected to be helpful to the film manufacturers in predicting film's final properties by omitting the dependency on post-production qualification procedures, reducing the film's quality inspection time and optimize the processing parameters accordingly. Several key research objectives need to be addressed to achieve the main aim and they are;

- (1) To establish digital image correlation as a deformation measurement tool in plastic film blowing process.
- (2) To comprehend the degree of deformation and structural changes during formation of bubble and film formed during plastic film blowing process.
- (3) To evaluate the shrinkage deformation response using DIC as a function of shrinkage temperature and processing parameters.
- (4) To analyse the combination effect of film strain and molecular structure on film mechanical properties; tensile and impact.

1.4 Thesis Outline

Thesis is organized into five chapters and the role of each chapters is explained as below;

Chapter 1 introduces briefly the background of the research, research motivation and its contribution, along with the objectives of the research.

Chapter 2 explains the fundamental of the film blowing process and digital image correlation analysis. It also reviews the previous research studies about

conventional strain measurement methods and applications of DIC in polymer processing.

Chapter 3 describes the experimental works carried out during the research study which includes the materials, equipment and procedures for each experimental method.

Chapter 4 discusses all the results and findings achieved from this research work. Section 4.1 discusses the feasibility of the DIC in film blowing process by studying the marker type that can be applied on film surface and validation of the DIC analysis. Section 4.2 discusses the influence of DIC parameters on the measurement accuracy. Section 4.3 confers thermal properties of high-density polyethylene (HDPE). This section also presents the bubble temperature, deformation and structural development during bubble formation; exiting the die to above freeze line height. Section 4.4 discusses the thermal properties, bubble temperature, deformation and structural development of films formed as a function of blow up ratio and take up ratio. Section 4.5 discusses the comprehensive shrinkage deformation through DIC method as a function of shrinkage temperature and processing parameter. Section 4.6 discusses the combined effect of the strain and molecular structure on film properties; tensile and impact.

Chapter 5 presents main findings form this research work and few recommendations for future research.

CHAPTER 2

LITERATURE REVIEW

2.1 Film Blowing Process

Film blowing extrusion is one of the commercial process in the manufacturing of high-volume of polymeric film (Gururajan and Ogale, 2012). Plastic bags and films of varying sizes are produced with this process. Mostly, different types of polyethylene (high-density polyethylene, low-density polyethylene, linear low-density polyethylene, metallocene linear low-density polyethylene) are processed and in certain applications, polymers such as polyamide, polyethylene terephthalate and ethylene-vinyl alcohol copolymer are processed as well.

The basic plastic film-blowing process is illustrated Figure 2.1. The process involves melting the polymer above its melting temperature and extruding through an annular die to form a tube. The tube is blown into a bubble with larger diameter and pulled upwards against the direction of gravitational force by the take up rolls. External air stream is used to cool and solidify the bubble (Troisi et al., 2016, Lee et al., 2015). During solidification process, the film crystallizes and rearranges to their preferred orientation from entangled amorphous melt into a semi-crystalline state. Solidification occurs at a point called as freeze line height where a ring-shaped region of frosty appearance formed on the film surface due to the reduction in temperature from melting to room temperature. This is the transition point between melt and solid phases and is assumed that negligible deformation of bubble will take place beyond this point (Kolarik et al., 2013, Pirkle and Braatz, 2011). The blown and solidified film is flattened by passing through the take up rolls and wound as double-layered plastic rolls.

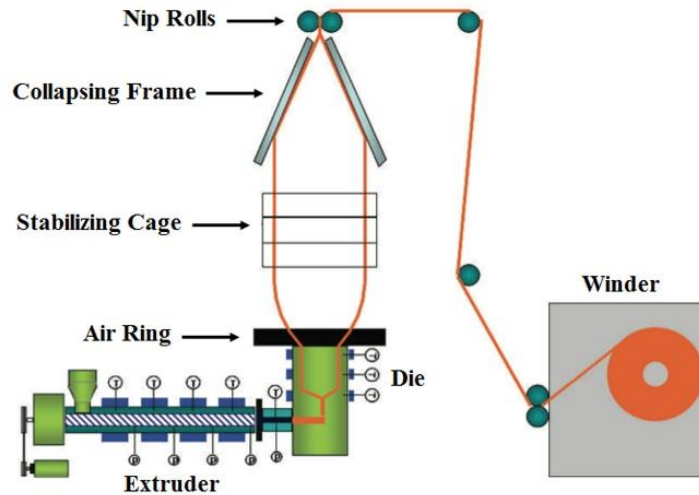


Figure 2.1 Film blowing extrusion process (Wagner, 2016)

The bubble experiences simultaneous biaxial stretching in axial (machine) and circumferential (transverse) directions that imposes selective molecular orientation and controls the mechanical properties of film. The circumferential stretching is influenced by the processing parameter known as blow up ratio (BUR) affected by air pressure inside the bubble. The axial stretching is manipulated by take up ratio (TUR) that is caused by the drawing force of the nip rolls (Pirkle and Braatz, 2010, Hyun et al., 2004).

Blow up ratio (BUR) is the ratio of the final bubble diameter to the die diameter. As the process is continuous, it is difficult to measure the final bubble diameter. Thus, the BUR is rearranged as the ratio between $0.637 \times$ lay-flat width and die diameter. The BUR increases as the air pressure inside the bubble increases and expands the bubble volume. This causes the melt to be stretched and oriented in transverse direction causing lamella disorder in machine direction. The higher the BUR, the thinner the film and the lower the freeze line height that cools the bubble quicker (Kolarik and Zatloukal, 2011, Auksornkul et al., 2018).

Take up ratio (TUR) is defined by the velocity gradient between velocity above freeze line and velocity of the melt at die exit. The TUR increases as the speed of the nip rolls increases triggering the melt to be stretched more in the machine direction. As a consequent, the lamellae perfectly stack and the amorphous chains orient in the machine direction. The speedier the nip rolls, the higher is the height of freeze line and the thinner the film (Kolarik and Zatloukal, 2011, Zhang et al., 2018a).

2.2 Microstructural deformation

Microstructural deformation of semi-crystalline polymers during film blowing process is controlled by the processing temperature and the stress imposed to orient the polymer chains. The semi-crystalline polymers have their ability to form some portion of ordered arrangement of crystalline region within the disordered amorphous regions. The crystalline region is responsible to the degree of crystallinity. The amorphous region comprises of randomly entangled polymer chains with tie chains and loose chain ends (cilia) that comes from the crystalline lamella. The ties chains in amorphous are formed between two different lamellae compared to cilia which is connected to only one lamella (Men and Rieger, 2003).

Chains that are free from crystalline region is known as mobile amorphous. In contrast, polymer chains at the interface between crystalline and amorphous is called rigid amorphous because the mobility of these chains is constrained by the adjacent crystalline region (Sedighiamiri et al., 2014, Jabbari-Farouji et al., 2017). This eventually will disrupt the capability of the polymer chains to orient properly and prevents the crystallisation (Androsch et al., 2010). A simple illustration of the randomly entangled polymer chains that strongly linked to the neighbouring

crystalline region through tie chains and cilia in semi crystalline polymer (Wietzke et al., 2010) is represented in Figure 2.2.

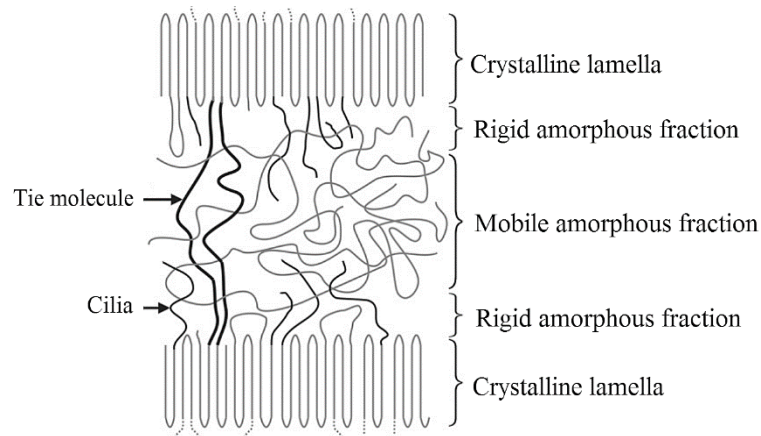


Figure 2.2. Structure of semi-crystalline polymers consisting of crystalline and amorphous regions (Wietzke et al., 2010)

The morphology of semi-crystalline polymer under flow is different from the quiescent conditions. Under quiescent conditions or the unstressed state, polymer chains in the molten state appear with random configuration without any orientation. They form a huge number of different conformations which is temporary and changes rapidly in a very short period of time. The un-stretched chains nucleate and grow forming crystals of chain-folded lamellae called as spherulite upon cooling, illustrated in Figure 2.3 (Nitta, 2016, Saeidijavash et al., 2017).

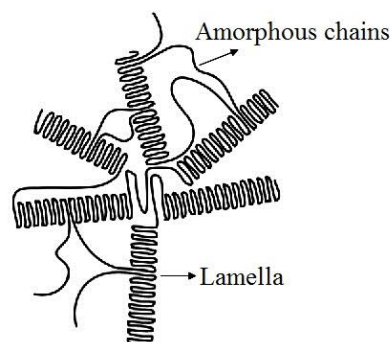


Figure 2.3 Randomly oriented polymer chains under un-stressed state (Saeidijavash et al., 2017)

Meanwhile, the polymer chains under flow causes orientation and stretching in the direction of flow and form shish-kebab structure or row-nucleated structure. The row-nucleated structure proposed by Keller and Machin (1967) is commonly used to explain the crystalline structure of blown polyethylene films under stress, depicted in Figure 2.4. The stretched chains are oriented in the flow direction (MD) and act as nucleation site. From the nucleation site, the folded chain lamellae grow radially in normal direction to MD and forms stacks of lamellae (Dargazany et al., 2014, Zhang et al., 2018b).

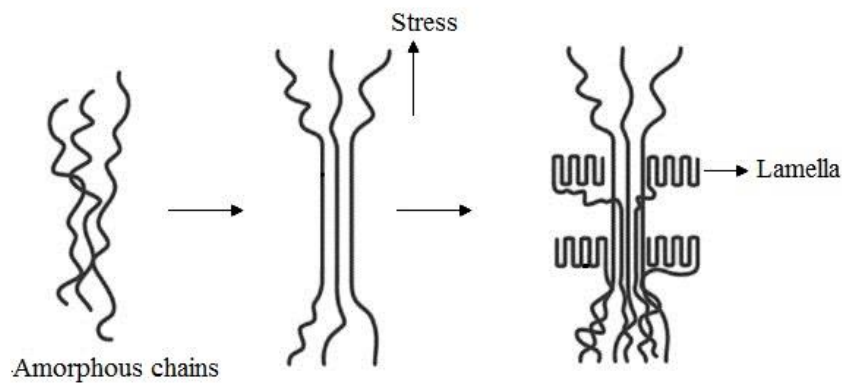


Figure 2.4 Row-nucleated structure of polymer chains at stressed state (Dargazany et al., 2014)

During the film blowing extrusion process, the molten polymer experiences different stresses before and after exiting the die. The melt is exposed to shear stress flowing through the die causing partial molecular orientation in the flow direction. During this time, rapid nucleation and growth takes place creating more tie chains in amorphous joining the lamellae of the same stack (Peterlin, 1971). Upon leaving the die, the melt experiences elongational stress that pulls the melt upwards and stretches biaxially to impart further extension and orientation to the polymer chains (Tabatabaei et al., 2009, Yamamoto, 2009).

The degree of polymer chain's orientation is influenced by the rate of stretching in both machine and transverse direction which can be modified by manipulating processing parameters. Smaller stretching rate causes fewer changes in polymer orientation, whilst, the chains shows almost fully oriented conformation once the critical stretching rate has reached (Zuidema, 2000).

2.3 In-plane Deformation

Deformation, displacement and strain are key factors in continuum mechanics. Strain is a measure of deformation that describes the displacement between points in a material relative to a reference length. The reference length can be the initial length before deformation or the length after deformation. The common strain definitions are engineering, logarithmic, Lagrangian and Eulerian strain, written as in Equation 2.1 and Equation 2.4.

Deformation can be grouped based on the extent of strain, infinitesimal or finite deformation (Hashiguchi and Yamakawa, 2012). Infinitesimal deformation involves small displacement and strain that is sometimes negligible. Concrete and steel in civil engineering application can be taken as an example, where the deformed and undeformed configuration of the material is indistinguishable. Commonly engineering strain is used for infinitesimal deformation as the logarithmic, Lagrangian and Eulerian strain eventually reduces to engineering strain.

Finite deformation deals with large displacement and strain. The material configuration before and after deformation is obviously distinguishable as such in polymers. For instance, polymers experience large deformations that is usually greater than 1% of an engineering strain. Engineering strain is not preferred for large strain

measurement, and typically Lagrangian and Eulerian strains are employed. Lagrangian strain is defined as change in squared root of material with respect to the initial length and orientation and, preferred in solid mechanics. Eulerian strain gives the change in squared root of material in terms of the final length and orientation and, preferred in gaseous or fluid mechanics (Dimitrienko, 2011). These definitions are written as in Equation 2.3 and Equation 2.4.

$$\text{Engineering strain} = \frac{l-l_0}{l_0} \quad (2.1)$$

$$\text{Logarithmic strain} = \ln \left(\frac{l}{l_0} \right) \quad (2.2)$$

$$\text{Lagrangean strain} = \frac{1}{2} \left(\frac{l^2-l_0^2}{l_0^2} \right) \quad (2.3)$$

$$\text{Eulerian strain} = \frac{1}{2} \left(\frac{l^2-l_0^2}{l^2} \right) \quad (2.4)$$

In film blowing practices, it processes viscoelastic polymer that shows both fluid (viscous component) and solid (elastic component) mechanics aspects, thus both the Lagrangian and Eulerian strains can be taken into consideration. However, the Lagrangian strain is preferred as the polymer is treated as solid in the film processing. The deformation of the film is obtained with the respect to the material position at the die exit rather than the final stretched film position that occupied temporarily. Smith and Stolle (2002) investigated and compared the application of Lagrangian and Eulerian strain to explain the film casting process. It was concluded that Lagrangian definition is more practical than the Eulerian as it can go for more complex problems that include the addition of two-dimensions, complex viscoelastic and non-isothermal effects.

2.4 Digital Image Correlation

Digital image correlation (DIC) is an optical system applied in measuring the full-field displacements and strains on a surface of object that is subjected to a progressive deformation object using non-contact mode. Digital image correlation is broadly recognized and practiced in solid mechanics such as polymers, woods, metals, biological mechanical, composite material, concrete, biological materials, etc.

The experimental set-up of DIC in any application is relatively simple which comprises of a test sample, camera and a light source. Special care should be given in the arrangement of the three components to get an accurate and consistent deformation measurement. The diagrams of simple experimental set-up using the test sample, light source and camera for two dimensional DIC (2D-DIC) and three dimensional DIC (3D-DIC) are displayed in Figure 2.5. Two-dimensional deformation studies use a single camera to determine in-plane displacement of planar surface. Some deformations involve non-planar surfaces with three dimensional geometries which require multiple cameras or one/two cameras with stereovision configuration of 3D-DIC analysis (Sutton et al., 2009, White et al., 2017, Sutton et al., 2008, Wu et al., 2016).

In year 1982, DIC was first projected to estimate the surface displacements components using continuum based matching principle in laser speckle metrology by Peters and Ranson (1982). It is followed by Sutton et al. (1983) that documented a non-linear least square principle using first order gradients as a matching function to find displacements and successfully implemented to analyse displacement of a cantilever beam with an end load. DIC has been developed and improved continuously based on the computational efficiency and measurement accuracy (Vendroux and

Knauss, 1998, Lu and Cary, 2000, Zhou and Goodson, 2001, Cheng et al., 2002, Yoneyama and Morimoto, 2003, Pan et al., 2009b, Pan and Li, 2011), and the research is still progressing. A few commercial DIC GOM-Correlate, Vic-Correlated Solutions and, open-sources software such as NCORR (Blaber et al., 2015), Multi-DIC, (Solav et al., 2018), and DICe (Turner et al., 2015) are available to perform DIC analysis. Besides, DIC software can be programmed dedicated to specific application if the principle of operation is well understood.

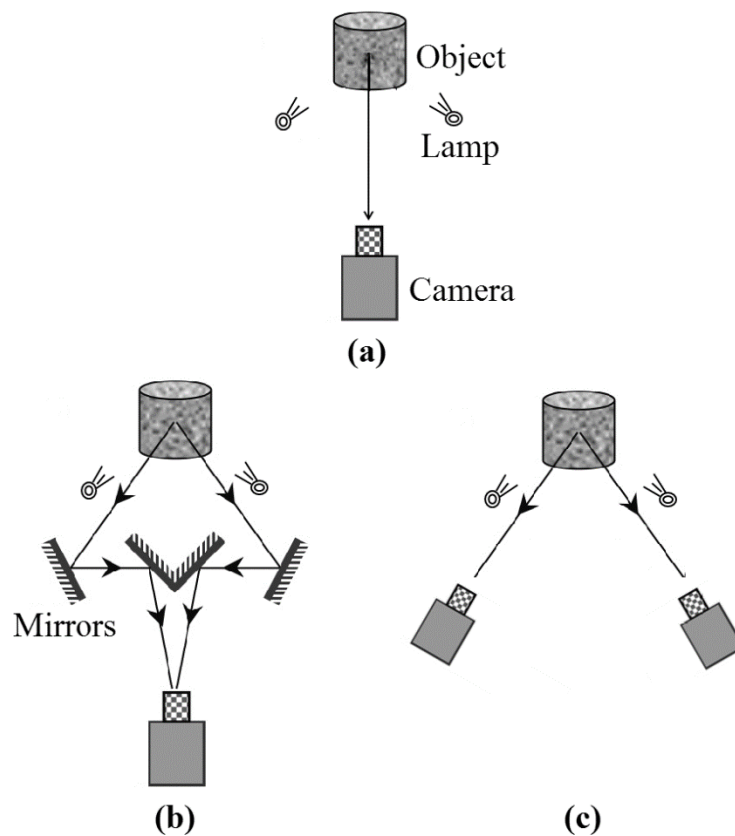


Figure 2.5. Experimental set-up (a) 2D-DIC; stereo-vision 3D-DIC using (b) single camera and set of mirrors (c) two camera (Pan et al., 2017)

2.4.1 Basic Principle of Digital Image Correlation

The Digital Image Correlation (DIC) is a simple principle operates by mathematically comparing the value of grayscales on images taken at two different states; un-deformed (reference) and deformed (current). For this purpose, the object at reference state required to have some features that holds grayscale values in the image to signify the deformation. It is assumed that after deformation, the pixel and the surrounding pixels in reference image are found in the current image(s) as well, meaning both images have comparable grayscale values.

Figure 2.6 shows the displacement of coordinate before and after deformation and, their deformation parameters (Khoo et al., 2016). The displacement of the coordinate from the reference point (x, y) to the current point (x^*, y^*) is based linear first order transformation mapping function and written as in Equation 2.5 and Equation 2.6.

$$x^* = x + u_x + \frac{\partial u_x}{\partial x} \Delta x + \frac{\partial u_x}{\partial y} \Delta y \quad (2.5)$$

$$y^* = y + u_y + \frac{\partial u_y}{\partial x} \Delta x + \frac{\partial u_y}{\partial y} \Delta y \quad (2.6)$$

where u_x and u_y represents the displacement elements at the centre of the subset, Δx and Δy represents the distance elements from the centre of the subset to a point (x,y) and $\frac{\partial u_x}{\partial x}$, $\frac{\partial u_x}{\partial y}$, $\frac{\partial u_y}{\partial x}$ and $\frac{\partial u_y}{\partial y}$ are the displacement gradients. The displacements are determined by searching the set of displacements; two unknown displacement components and the four displacement gradients that are obtained through the correlation process.

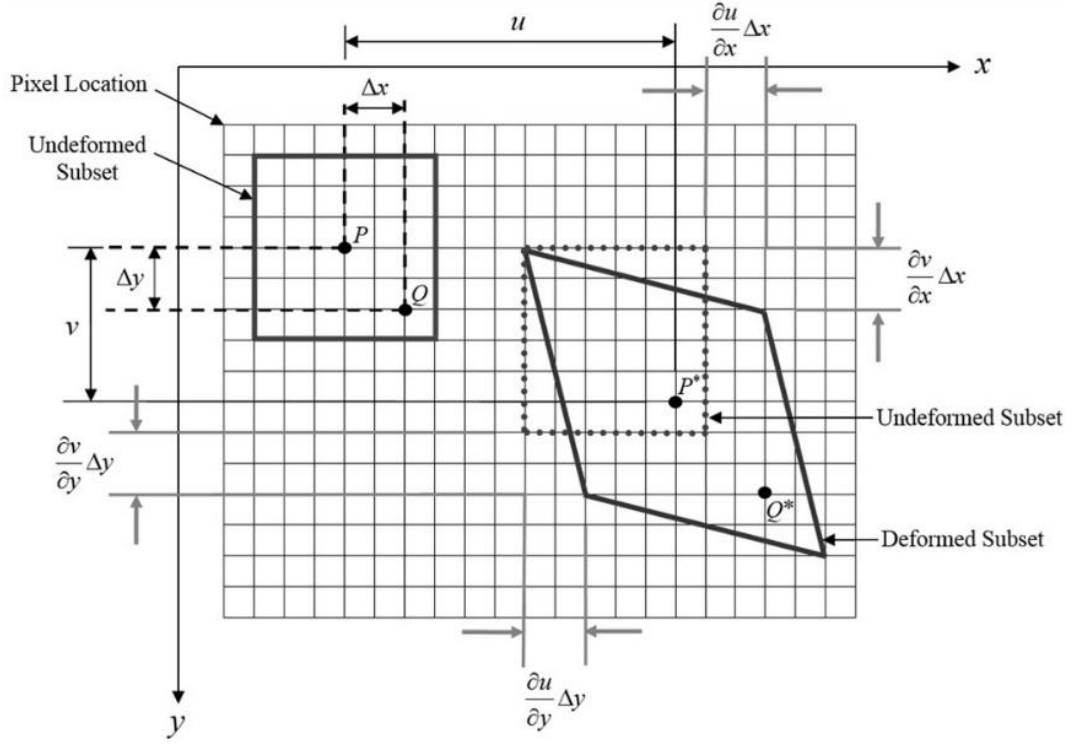


Figure 2.6. Diagrams illustrates the displacement coordinates before and after deformation and the deformation parameters (Khoo et al., 2016)

Zero-Normalised Cross-Correlation Criterion (ZNCC) and Zero-Normalised Squared Sum of Differences Criterion (ZNSSD) are testified as the optimum correlation criterion to find the similarity between the images. The ZNCC and ZNSSD correlations are favoured as the accuracy of the results obtained is not sensitive to the light variations (Pan, 2009, Hassan et al., 2016). The equations for ZNCC, ZNSSD and their relations are written as in Equation 2.7, Equation 2.8 and Equation 2.9, respectively. The mean grayscale intensity, f_m (reference) and g_m (current) are described as in Equation 2.10 and Equation 2.11, correspondingly (Blaber et al., 2015).

$$\text{ZNCC} = \frac{\sum_{(i,j) \in S} (f(x_i, y_j) - f_m) (g(x_i^*, y_j^*) - g_m)}{\sqrt{\sum_{(i,j) \in S} [f(x_i, y_j) - f_m]^2 \sum_{(i,j) \in S} [g(x_i^*, y_j^*) - g_m]^2}} \quad (2.7)$$

$$\text{ZNSSD} = \sum_{(i,j) \in S} \left[\frac{f(x_i, y_j) - f_m}{\sqrt{\sum_{(i,j) \in S} [f(x_i, y_j) - f_m]^2}} - \frac{g(x_i^*, y_j^*) - g_m}{\sqrt{\sum_{(i,j) \in S} [g(x_i^*, y_j^*) - g_m]^2}} \right]^2 \quad (2.8)$$

$$ZNCC = 1 - 0.5 \times ZNSSD \quad (2.9)$$

$$f_m = \frac{\sum_{(i,j) \in S} f(x_i, y_j)}{n(S)} \quad (2.10)$$

$$g_m = \frac{\sum_{(i,j) \in S} g(x_i^*, y_j^*)}{n(S)} \quad (2.11)$$

where, f and g are grayscale intensity functions of the reference and current image at a specified location (x,y) , reference point (x, y) to the current point (x^*, y^*) . Function f_m and g_m represent the mean grayscale values of reference and current image. $n(S)$ is total data points in subset S .

The ZNCC is used to find the initial guess that yields the u and v with integer (pixel) accuracy and ZNSSD to refine these results with sub-pixel resolution accuracy. Once the best resemblance is found, the displacement components of the reference and current subset centres can be determined. The displacement components are used to compute the displacements and their corresponding strain (Yoneyama, 2016, Hassan et al., 2016, Pan, 2018). The strains can be calculated in u direction and v direction with respect to E_{xx} , and E_{yy} as in Equation 2.12 and Equation 2.13.

$$\varepsilon_{xx} = \frac{1}{2} \left[2 \frac{\partial u_x}{\partial x} + \left(\frac{\partial u_x}{\partial x} \right)^2 + \left(\frac{\partial u_y}{\partial x} \right)^2 \right] \quad (2.12)$$

$$\varepsilon_{yy} = \frac{1}{2} \left[2 \frac{\partial u_y}{\partial y} + \left(\frac{\partial u_x}{\partial y} \right)^2 + \left(\frac{\partial u_y}{\partial y} \right)^2 \right] \quad (2.13)$$

2.4.2 Aspects of Measurement Accuracy

Digital image correlation able to measure the displacement and strain accurately if the care is given during pre-processing and post-processing the DIC analysis.

2.4.2(a) Pre-processing

Preparation of the sample surface with a proper surface pattern and the lighting condition is essential before proceeding with recording and capturing the reference image for the DIC analysis. A surface pattern is essential in DIC analysis because it provides distinctive grayscale variations to track and correlate the location of subset from reference image to current image upon deformation. The surface pattern can be inherent surface texture or artificially created random pattern. In most case, the objects are in the absence of natural surface texture, hence, an artificial pattern is applied. The created patterns can be in the forms of dots, lines or random patterns and required to be isotropic and non-periodic appearance. A repeating and comparable orientation causes a faulty correlation that affects the DIC result. Artificial surface patterns can be created using techniques such as marked by pen, airbrush guns, via computer graphic manipulation and screen printing, spray paint, and so on. Care should be taken in choosing the correct technique for creating the pattern as the technique it is very dependent on the texture of the application (Tekieli et al., 2017, Khoo et al., 2016, Take, 2015). The detailed description on the creation of artificial patterns and their evaluation can be found in several literature (Crammond et al., 2013, Park et al., 2017, Mehdikhani et al., 2016, Giacomo Lionello and Luca Cristofolini, 2014).

Proper lighting within the testing environment is important. A small variation in the light intensity within the surface of sample will affect the measurement accuracy. Therefore, the surface of testing sample should be brightened with consistent light intensity throughout the deformation and recording process (Tekieli et al., 2017, Take, 2015).

2.4.2(b) Post-processing

A balance in selecting the DIC parameters such as subset size, subset space and strain radius are required to avoid errors in the calculation and enhance the measurement accuracy. Subset consists of speckles with varied grayscale values that used to track and correlate the similar pixels in the reference and current images. Commonly, a square shaped subset is used in the DIC analysis to find the best match of the reference image in current image (Pan et al., 2012, Pan et al., 2006, Pan, 2009). Meanwhile, studies using circular shaped subset also have been testified by Blaber *et al.* (2015). Subset size selection is a user input parameter and should be carefully chosen corresponding to the image size, pattern and mode of deformation of testing objects. Subset size is chosen by trying different subset sizes across the entire image to determine the optimum subset size for the DIC analysis. Larger subset size is favoured for heterogeneous deformation, whilst, smaller size for homogenous deformation (Park et al., 2017).

Subset space is the distance among two successive pixels inside a subset. Subset with smaller subset space contains more data points for correlation and vice versa. Subset space influences the image spatial resolution and the speed of calculation. Large subset space has lesser data points which diminishes the resolution

between the points, blurring the image and speed up the calculation process (Palanca et al., 2016, Wang et al., 2012). Smaller subset space is favoured for heterogeneous deformation and larger subset space for homogenous deformation (Sutton et al., 2009).

Strain values obtained from the DIC analysis do not perfectly represent the real strain values. High level of noises is present in the displacement fields, thus, a strain radius is essential to remove the undesirable noises (Pan et al., 2007). Large strain radius is desired for homogeneous deformation. For heterogenous deformation, the strain radius should be sufficiently small to avoid data smoothing but large enough to avoid noise in displacement data (Blaber et al., 2015).

2.5 Conventional Strain Measurement

Physical gauges such as extensometer and electrical resistance strain gage and, non-contact optical methods such as traditional video tracing method are widely explored and used in the deformation and strain measurement of polymer samples.

2.5.1 Physical Gauge Measurement

Extensometer can give a very reliable and accurate measurement. It is easy to place on samples and accessible in variety of sizes and holders to accommodate the type of the sample. Unfortunately, the sample on the extensometer can still slip from the sample holder or also, produces undesirable stress concentration at the sample and holder connection points (Brinson and Brinson, 2015, Jerabek et al., 2010, Tao and Xia, 2005). The electrical resistance strain gauges also able to provide accurate and precise readings of surface deformation measurement. However, it is very challenging to handle and must be cautiously fixed to the sample surface as it can be affected by

factors such as thermal or reinforcement (Brinson and Brinson, 2015, Jerabek et al., 2010).

Unfortunately, these tools are very challenging to be used in strain measurement of plastic in film blowing process where the film moves upwards at a relative speed while being stretched and deformed. These tools need to be carefully attached on the sample surface which tends to damage the film surface by creating undesirable local stress concentration points and stiffness. Even though, there is a possibility to place the tools outside the sample surface, but that will restrict the measurement to the strain gauge position and will require more strain gauges. Multiple number of strain gauges will affect the accuracy of the measurement. Irrespective to the gauge's placement (attached to surface or outside), it provides displacement and strain information on few discrete locations, difficult to calculate strain variation along the width and length of sample, identify the critical strain location and unable to study the complete deformation. Overall, these two tools (extensometer and electrical resistance strain gauge) are less favourable due to their complexity and poor measurement accuracy in real practise of plastic film blowing process. Table 2.1 lists out the research work of conventional measuring tools and its limitation and, compares with DIC that overwhelms such limitation in polymer characterisation.

Table 2.1 Conventional measuring tools vs DIC

Reference	Aim	Sample	Application/ Testing	Measuring tool & Limitations	Advantage of DIC
(Hua et al., 2007)	<ul style="list-style-type: none"> To study mechanical properties of low-dimensional materials using newly developed micro-tensile system. 	<ul style="list-style-type: none"> Polyethylene oxide film containing 15% nano-composite SiO₂ 	<ul style="list-style-type: none"> Micro-tensile test 	<ul style="list-style-type: none"> Displacement sensor/ Extensometer - Limited data on deformation which affects the measurement accuracy 	<ul style="list-style-type: none"> Provides full-field displacement and strain data
(Heinz and Wiggins, 2010)	<ul style="list-style-type: none"> To investigate uniaxial compression properties of epoxy resin. 	<ul style="list-style-type: none"> Epoxy 	<ul style="list-style-type: none"> Compression test 	<ul style="list-style-type: none"> Extensometers/Strain Gages - Small sample size and limited space 	<ul style="list-style-type: none"> Sensitive to small strain measurement
(Jerabek et al., 2010)	<ul style="list-style-type: none"> To compare DIC and mechanical extensometer in determining strain field in pre and post-yield of PP and PP composites under uniaxial tensile test. 	<ul style="list-style-type: none"> Polypropylene (PP) & PP composites 	<ul style="list-style-type: none"> Uniaxial tensile test 	<ul style="list-style-type: none"> Mechanical extensometer - Attached to surface (clip-on stress by pins) 	<ul style="list-style-type: none"> Non-contact and non-destructive
(Dong et al., 2017)	<ul style="list-style-type: none"> To investigate full-field thermal deformation and calculate coefficient of thermal expansion (CTE). 	<ul style="list-style-type: none"> Carbon fibre-epoxy composites 	<ul style="list-style-type: none"> Thermal expansion test 	<ul style="list-style-type: none"> High temperature strain gauge Fabrication, preparation, and attachment is costly, time-consuming and difficult. 	<ul style="list-style-type: none"> Full-field thermal deformation, high accuracy and cost effective.